

A high-efficiency programmable modulator for extreme ultraviolet light with nanometre feature size based on an electronic phase transition

Received: 29 March 2023

Accepted: 9 January 2024

Published online: 02 February 2024

 Check for updates

Igor Vaskivskiy¹✉, Anze Mraz^{1,2}, Rok Venturini^{1,3}, Gregor Jecl^{1,3}, Yevhenii Vaskivskiy^{1,3}, Riccardo Mincigrucci⁴, Laura Foglia⁴, Dario De Angelis⁴, Jacopo-Stefano Pelli-Cresi⁴, Ettore Paltanin⁴, Danny Fainozzi⁴, Filippo Bencivenga⁴, Claudio Masciovecchio⁴ & Dragan Mihailovic^{1,5}

The absence of efficient light modulators for extreme ultraviolet (EUV) and X-ray photons considerably limits their real-life application, particularly when even slight complexity of the beam patterns is required. Here we report on a novel approach to reversible imprinting of a holographic mask in an electronic Wigner crystal material with a sub-90-nm feature size. The structure is imprinted on a sub-picosecond timescale using EUV laser pulses, and acts as a high-efficiency diffraction grating that deflects EUV or soft X-ray light. The imprinted nanostructure is stable after the removal of the exciting beams at low temperatures, but can be easily erased by a single heating beam. Modelling shows that the efficiency of the device can exceed 1%, approaching state-of-the-art etched gratings, but with the benefit of being programmable and tunable over a large range of wavelengths. The observed effect is based on the rapid change of lattice constant upon transition between metastable electronically ordered phases in a layered transition metal dichalcogenide. The proposed approach is potentially useful for creating tunable light modulators in the EUV and soft X-ray spectral ranges.

In the past century, the range of useful wavelengths of coherent radiation was greatly extended from the infrared, visible and ultraviolet to the extreme ultraviolet (EUV), soft- and hard X-rays. Although in the optical range it is possible to effectively manipulate the spectral, temporal or spatial content of light using various passive (lenses, mirrors, diffraction gratings) and active (acousto- and electro-optic modulators, spatial light modulators (SLMs) and so on) elements, this becomes a

challenging task for high-energy photon beams. Several approaches can be used to produce EUV and X-ray diffraction gratings, such as lithographic etching of thin-film transmission gratings¹, or designing special multilayer blazed gratings². However, the working spectral range of these devices is usually relatively narrow and their manufacturing is a technologically complicated task due to the need for precise control over the etching process.

¹Jozef Stefan Institute, Department of Complex Matter, Ljubljana, Slovenia. ²Faculty for Electrical Engineering, University of Ljubljana, Ljubljana, Slovenia.

³Faculty for Mathematics and Physics, University of Ljubljana, Ljubljana, Slovenia. ⁴Elettra Sincrotrone Trieste, Trieste, Italy. ⁵CENN Nanocenter, Ljubljana, Slovenia. ✉e-mail: igor.vaskivskiy@ijs.si

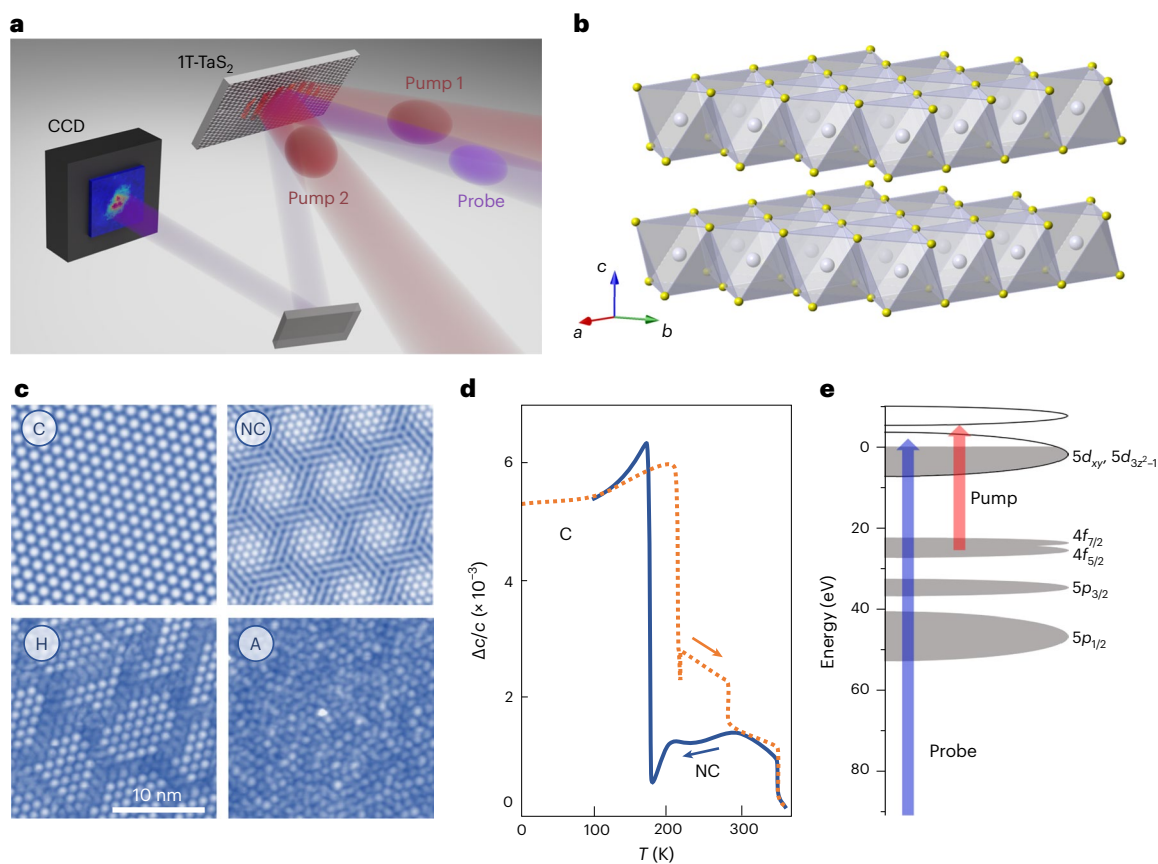


Fig. 1 | Scheme of the experiment and properties of 1T-TaS₂. **a**, The optical layout showing the EUV write beams (pumps 1 and 2) and the probe beam. CCD, charge-coupled device. **b**, The crystal structure of 1T-TaS₂. **c**, A schematic representation of the electronic ordering in the thermodynamic commensurate (C) and nearly commensurate (NC) CDW states, and the photoinduced states

H and A. **d**, The lattice expansion along the *c*-axis (after Sezermann et al.²²) for cooling (blue) and heating (orange) cycles. **e**, An energy-level diagram showing the pump and probe transitions. The assignments are from Ettema and colleagues²³.

Temporal modulation of the X-ray beam is usually performed by mechanically moving one or more optical elements in the beam path. Such an approach is cumbersome, has limited speed and precision, and is not always possible due to geometrical constraints. A miniature microelectromechanical system (MEMS) was presented recently, exhibiting a 350 MHz modulation frequency³. However, there are complications with the proposed device: its working frequency has to be matched to the repetition rate of the light source and it requires a beam with a small footprint, which might limit the total photon throughput. A new proof-of-principle device based on the phase-change material Ge₂Sb₂Te₅ was proposed for a reflective SLM in the X-ray spectral range⁴. Although demonstrating a fast 'writing' speed and high stability, this device suffers from a rather large feature size, limited by the heat propagation effects and the thermal nature of the switching process.

Here we demonstrate a novel approach that can be used as a reflective SLM for the EUV or soft X-ray beams; this approach features ultrafast switching time and a sub-90-nm feature size. For the proof-of-principle demonstration, we use two crossed coherent EUV beams (write beams) to imprint a metastable periodic structure into the electronically ordered quantum material 1T-TaS₂, in which the lifetime of the electronic state is controllable⁵ (Fig. 1a). This results in a diffraction grating, which efficiently deflects the short wavelength photons.

Transient gratings, which are formed by the interference of non-collinear pulsed visible or infrared laser beams interacting within a material, are commonly used to investigate carrier diffusion and lifetimes^{6–8}, heat propagation effects^{9,10}, acoustic waves^{11,12}, phonon polaritons^{13,14}, and electron-, vortex¹⁵ and spin-dynamics^{16–18} in a

wide range of materials. The EUV transient grating approach was recently demonstrated at the Fermi free electron laser (FEL) source^{19–21}. Such gratings are transient as they are limited by the non-equilibrium lifetime of the intrinsic excitations created in the material by the laser pulses. Typically heat dissipation, carrier diffusion or the charge-carrier recombination processes limit the grating lifetime to short timescales, usually not exceeding the nanosecond range. This can be overcome by the use of a metastable electronic state in 1T-TaS₂ with a tunable lifetime (from microseconds at 150 K to exceeding typical laboratory scales below 70 K; see ref. 5).

This material is a layered Van der Waals system (Fig. 1b) that exhibits a series of electronic ordering transitions and exotic metastable states in response to exposure to light. Under quasi-static thermodynamic conditions, the high-temperature metallic state develops an incommensurate charge density wave (CDW) at 550 K, which transforms to a unique 'nearly commensurate' state at 350 K that persists down to 180 K on cooling, whereupon it undergoes a first-order transition to a commensurate CDW. The nearly commensurate state is best thought of as a regular patchwork of commensurate domains separated by domain walls (Fig. 1c). A substantial change in lattice constants is associated with the nearly commensurate–commensurate transition²², namely, the out-of-plane expansion is particularly large and hysteretic (Fig. 1d).

Optical excitation of the commensurate state results in the formation of either a metastable chiral domain (H) state²³ or an amorphous (A) Wigner glass state²⁴, depending on the excitation parameters²⁵ (Fig. 1c). The lifetime of the 'hidden' H state, which is superficially

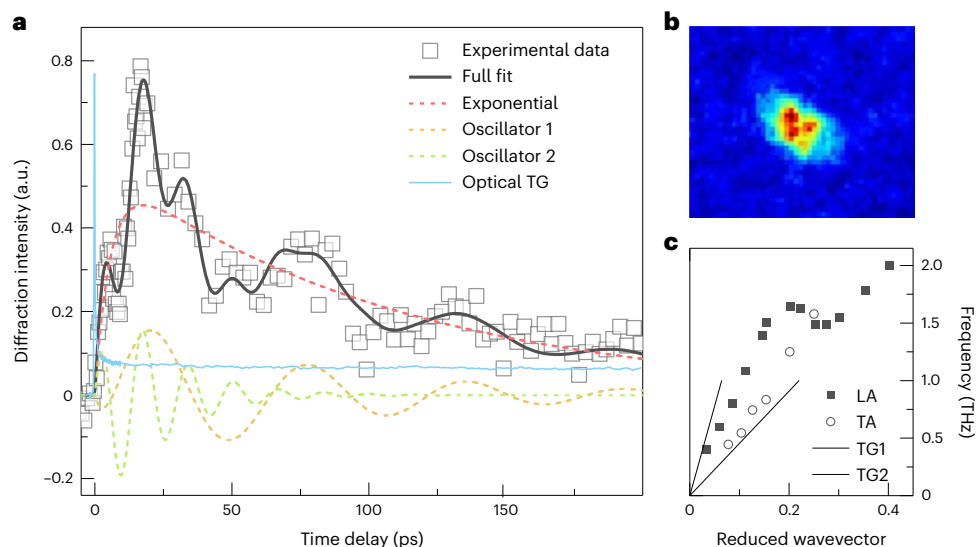


Fig. 2 | EUV transient grating measured at room temperature. **a**, The intensity of the probe beam diffracted from the EUV transient grating (TG) created by the write beams. The solid black line is the fit, the dashed lines are the separate components of the fit, and the solid blue line represents the optical pump–probe transient grating experiment. **b**, The footprint of the diffracted probe beam on

the CCD detector. **c**, The acoustic phonon velocities deduced from the grating period and oscillation frequency are indicated by the lines. The data points are the longitudinal scattering data (LA) and transverse acoustic (TA) phonon frequencies from neutron scattering data⁴⁰.

similar to a supercooled nearly commensurate order, can be conveniently controlled by temperature and strain⁵. The A state is more thermally robust than the H state and seems to exist on typical laboratory timescales up to at least 200 K (ref. 24).

In this work we show that the excitation of 1T-TaS₂ with two crossed EUV beams at low temperatures creates a metastable diffraction grating that deflects EUV light with remarkable efficiency. We also demonstrate that the imprinted structure can be erased with a single EUV beam, resulting in a programmable modulator for coherent EUV radiation. The extraordinarily high diffraction efficiency of the device is caused by the lattice contraction in an out-of-plane direction associated with the electronic phase transition.

Results and discussion

We study the device operation in a typical transient grating experimental configuration, focusing on the evolution of the electronic order in 1T-TaS₂ at two temperatures. First, we perform measurements at room temperature, where the ground state of the sample is a nearly commensurate CDW and no long-lived metastable state is expected. We observe a typical transient grating response on the picosecond timescale (Fig. 2a), which is driven by the nearly resonant pump with a photon energy of 31.1 eV, and probed away from any atomic transitions by 93.3 eV photons in backward diffraction geometry (Fig. 1a). The transient grating period was set to 87 nm. Typically for EUV, the signal consists of an exponential background with superimposed oscillations that originate from periodic modulation of lattice temperature²⁶. This is also confirmed by the rise time of the signal (5.2 ± 1 ps), which matches with the electron–lattice thermalization time²⁷. The relaxation rate, on the other hand, is given by the heat diffusion time in the system. The slower oscillation corresponds to the surface acoustic wave, with a frequency close to the transverse acoustic phonon (Fig. 2c), whereas the faster oscillation might be attributed to the surface skimming longitudinal wave with a frequency close to the longitudinal acoustic phonon. The transient grating signal almost completely disappears after 200 ps, signifying the thermal equilibration between the bright and dark grating fringes. The disappearance of the diffracted signal, however, does not necessarily mean the complete relaxation of the system to the ground (nearly commensurate) state. Earlier all-optical

studies²⁷ have revealed that at high excitation fluences the lattice might momentarily reach the incommensurate–nearly commensurate transition temperature, so it is plausible that the whole probed area of the sample is thermally converted into the high-temperature incommensurate state, which then relaxes back to the nearly commensurate state on a much longer timescale, once the heat is transported away. It is worth noting that due to non-resonant probe photon energy, we do not directly observe sub-picosecond change of electronic order²⁸. By contrast, in all-optical transient grating experiment, the fast electronic component is about ten-times stronger than the slower lattice response (cyan trace in Fig. 2a).

We next perform a similar experiment at 100 K, in which the ground state of 1T-TaS₂ is a commensurate CDW. At this temperature, the pulsed photoexcitation is known to create various metastable orders. Already after the first exposure to the crossed pump beams, a strong scattering appears on the detector at the wavevector of the transient grating. Remarkably, the scattering intensity was still present and almost constant even after the pump beams are blocked, revealing permanent imprinting of the periodic structure (Fig. 3), which does not relax for at least 750 s. After 750 s, the sample was excited by one of the EUV pump beams, which does not create an interference pattern in this case, but rather plays a role of a heating pulse. We show in Fig. 3b that this ‘erases’ the diffraction grating in 48 ± 3 s (exponential fit). After blocking the pump beam and allowing the sample to cool down, the whole process of semi-permanent switching can be repeated on the same spot of the sample, confirming that no degradation of the surface occurred.

We attribute the strong scattering signal with a long lifetime to a photoinduced phase transition to a metastable hidden electronic order^{23,24,27} (Fig. 3a): while the bright illuminated stripes in the EUV grating are converted to the photoinduced state, the dark areas stay in the ground state. The diffraction efficiency of the imprinted structure is at least one order of magnitude higher than the transient grating at 300 K. Such a stabilized structure would not be possible in the event of a thermal phase transition, in which case the temperature of the bright and dark stripes would equilibrate on a sub-nanosecond timescale and thus the whole sample would end up in a single phase, either a nearly commensurate or commensurate CDW depending on the final

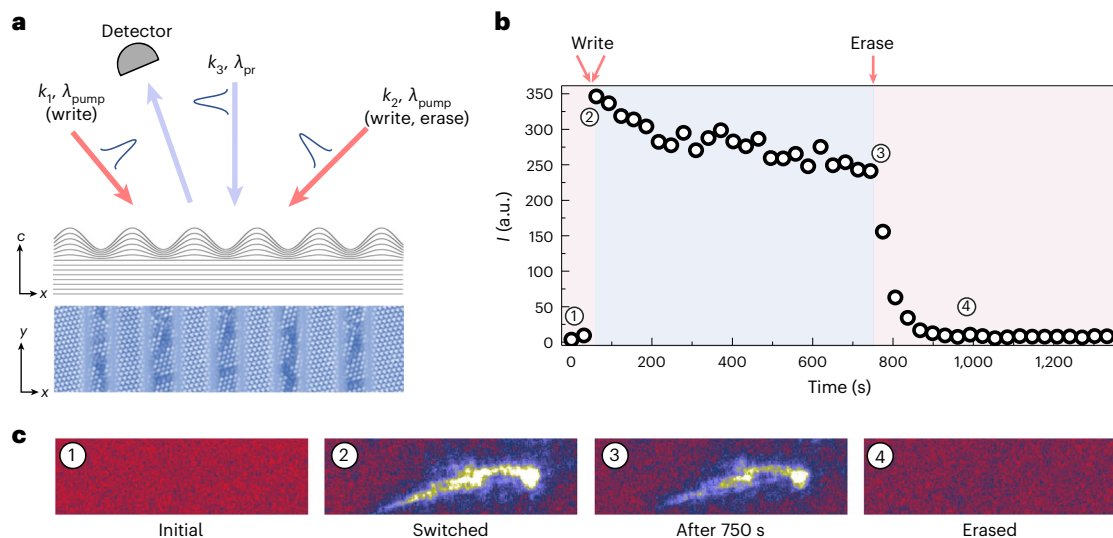


Fig. 3 | EUV diffraction observed at low temperature. **a**, A schematic diagram of the sample dilation along the *c*-axis caused by writing a grating onto the sample and the metastable periodic C/H structure. **b**, The intensity of the diffracted probe beam on the CCD as a function of time, with the timings of the write and

erase pulses indicated above. **c**, The diffracted streaks recorded on the CCD at the numbered data points in **b**: (1) initial state; (2) immediately after switching (3); 750 s after switching; and (4) after erasing the grating with a single EUV beam.

lattice temperature. The existence of a photoinduced hidden state is therefore essential for such a long-lived effect to occur. Although we do not have direct information on the type of the final state from the current data, judging from the high stability of the structure at 100 K, it is plausible that the A phase, or a mixture of the A and H states, is reached.

We note that the EUV light used in this work is very different from the traditional optical or electrical excitations; thus, it might not be possible to define the type of the photoinduced state solely on the basis of existing excitation fluence values, and systematic study of the switching efficiencies at different wavelengths is required to elucidate the phenomenon. In our experiment, the fluence in the bright fringes of the crossed pump beams reached 15.2 mJ cm^{-2} , which is much higher than the excitation fluences used in earlier optical switching experiments and—together with shorter absorption length of resonant EUV light—corresponds to ~30-times-higher energy density absorbed in the sample. On the other hand, the density of absorbed photons is comparable in the present case and earlier optical data.

Similarly to the room-temperature case, the diffraction signal at 100 K mainly originates from the periodic deformation of the lattice. The rather inhomogeneous shape of the diffracted signal observed in such a metastable configuration (Fig. 3c) can be attributed to a non-uniform heating and strain in partially cracked or detached flakes on the sample surface, which affects the stability of the photoinduced state²⁹ and causes its partial relaxation.

Two pathways for thermal erasing of the semi-permanent periodic structure with a single pump beam can be envisaged. First, if the fluence of the pump beam is above the switching threshold, then each individual pulse causes the whole sample to be converted into the photoinduced state. This would cause immediate disappearance of the diffracted signal. At later time, due to excessive direct current heating from the long pulse train, the sample might recover to the ground state. Second, if the fluence of the single pump beam is below the switching threshold, then the direct current heating of the sample is the only necessary process to be considered. The erasing time would depend on the heat load and the resulting sample temperature⁵.

As the diffraction intensity drops with a relatively long time constant ($48 \pm 3 \text{ s}$) in our experiment with a 3.8 mJ cm^{-2} pump, we conclude that the second scenario is operative.

To understand the unexpectedly high diffraction efficiency of the metastable structure, we have to consider the evolution of the crystalline lattice, which accompanies the electronic phase transition. The commensurate state is characterized by the unique ordering of the CDWs in the neighbouring layers which, among others, causes a ~0.5% change of the out-of-plane lattice constant when cooling from the nearly commensurate state (Fig. 1d). As the photoinduced states are characterized by nearly commensurate-like stacking^{30–32}, a jump of a similar magnitude can be expected also in the present case resulting in a real-space electronic and lattice modulation. This can be considered as a nearly sinusoidal reflective diffraction grating (Fig. 3a). Its efficiency can be estimated from³³:

$$\eta = \frac{I_d}{I_0} = R J_1^2 \left\{ \frac{a}{2} \right\},$$

where I_d and I_0 are diffracted and incident intensities, respectively, R is the reflectivity of the material, a is the peak-to-peak excursion of the phase, and J_1 is Bessel function of the first kind. In paraxial approximation $a = \frac{4\pi h}{\lambda}$, where h is the height of the surface modulation and λ is the photon wavelength. The resulting diffraction efficiency for 13.3 nm photons in our experimental geometry is $\eta_{\text{calc}} = 10^{-7}$, which matches well the experimentally measured value of $\eta_{\text{exp}} = 9.5 \times 10^{-8}$. Here, tabulated optical constants³⁴ were used for calculating the reflectivity of the sample and the thickness of the switched layer. Importantly, according to this simple modelling, by tuning the experimental geometry and impinging the laser beams at an oblique angle, it should be possible to enhance the efficiency of the grating by more than two orders of magnitude. The angular dependence of the diffraction efficiency for different photon energies is plotted in Fig. 4a. For shorter values of λ and at large incidence angles, the efficiency can be enhanced further, and for $\lambda = 0.5 \text{ nm}$, the calculated value reaches $\eta_{\text{calc}} = 0.1\%$. It is also worth noting that unlike the polished optical elements, the proposed device can be produced with an atomically flat surface owing to the layered structure of 1T-TaS₂.

Here we estimate the amplitude of the grating to reach $h = 0.1 \text{ nm}$, which is much larger than previously reported values for EUV transient grating³⁵. This parameter is responsible for the high diffraction efficiency of the structure and is defined by the relative change of the unit

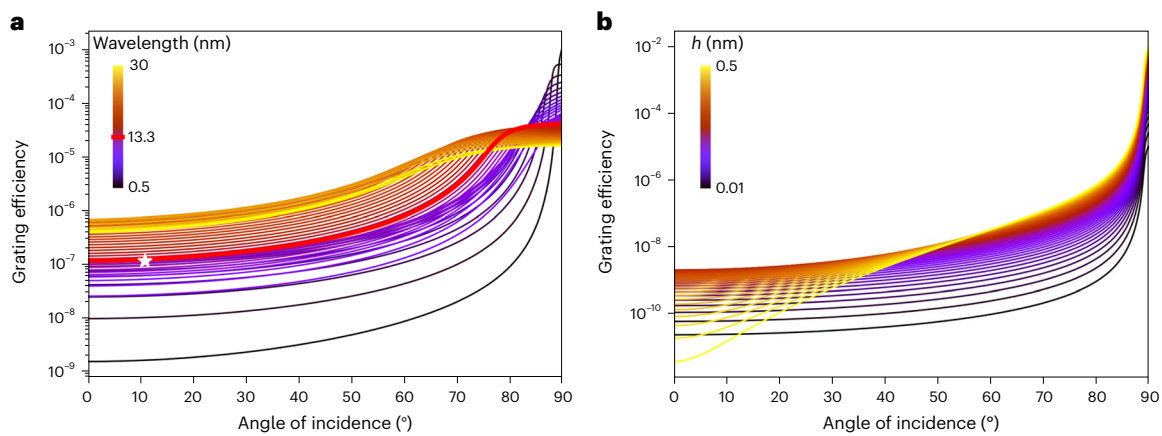


Fig. 4 | Modelling the efficiency of a sinusoidal grating. **a**, Calculated diffraction efficiency of the sinusoidal grating as a function of the angle of incidence for different wavelengths in the 0.5–30 nm range. The bold red line represents the modelling for the probe wavelength ($\lambda = 13.3$ nm) used in the

experiment, whereas the white star indicates the experimentally measured value. **b**, Calculated diffraction efficiency of the sinusoidal grating as a function of the angle of incidence for fixed wavelength ($\lambda = 0.5$ nm) and different modulation amplitudes in the 0.01–0.5 nm range.

cell at the phase transition and the attenuation length of the pump photons in the sample. By switching a thicker layer of the sample, it should be possible to reach $\eta_{\text{calc}} > 1\%$ (Fig. 4b) and thus approach the efficiencies of the state-of-the-art multilayer etched gratings ($\sim 5\%$)¹. In general, it might be beneficial to use shorter wavelength photons due to their longer absorption length; however, further investigation into the switching process at different atomic resonances and with non-resonant excitation is required to optimize the wavelength. By optimizing the experimental conditions and fine-tuning the balance between thermal and non-thermal effects, it might be also possible to change the duty cycle and spatial profile of the imprinted structure, which can help to redistribute the intensity between different diffraction orders. We expect that the feature size of the grating can be further decreased approaching the intrinsic domain size in the hidden state (10–20 nm). The phase transition was already successfully triggered in a 60 nm device by current injection³⁶.

Although we used bulk exfoliated crystals in this work, which is not a technologically scalable solution, recent developments in chemical vapour deposition^{37,38} molecular beam epitaxy³⁹ growth of thin 1T-TaS₂ might provide the prospects for industrial manufacturing of high-quality and large-area devices based on thin films.

Conclusion

We have created a programmable EUV and soft X-ray spatial light modulator in which the periodic structure can be written and erased on demand using short laser pulses. The unexpectedly large amplitude of the surface modulation arises from the large out-of-plane lattice contraction concurrent with the photoinduced phase transition. The stability of the structure is directly related to the long lifetime of the photoinduced hidden charge-ordered states in the material. The formation of the grating is not inherently limited to the present combination of wavelengths. An extension to other wavelengths would result in a wavelength-tunable and programmable grating for EUV and soft X-ray radiation.

Beyond the laser imprinting, which requires two crossed coherent EUV beams for 'writing the structure, a hybrid electro-optical device could be envisaged. In this case, the textured electronic structure could be created by current injection using an array of electrodes in a manner very similar to liquid-crystal-based SLMs. The presented tunable device can be also used as an intensity and spectral monitor, dispersing a small portion of the beam onto the reference detector. By varying the properties of the imprinted grating, it would be possible

to tune the usable spectral range and/or the spectral resolution of a spectrometer without the need to replace or mechanically move any component of the system, adding much more flexibility in EUV and soft X-ray optical layouts.

Online content

Any methods, additional references, Nature Portfolio reporting summaries, source data, extended data, supplementary information, acknowledgements, peer review information; details of author contributions and competing interests; and statements of data and code availability are available at <https://doi.org/10.1038/s41566-024-01389-z>.

References

- Wang, X., Kazazis, D., Tseng, L.-T., Robinson, A. P. G. & Ekinci, Y. High-efficiency diffraction gratings for EUV and soft X-rays using spin-on-carbon underlayers. *Nanotechnology* **33**, 065301 (2022).
- Voronov, D. L. et al. X-ray diffraction gratings: precise control of ultra-low blaze angle via anisotropic wet etching. *Appl. Phys. Lett.* **109**, 043112 (2016).
- Chen, P. et al. Optics-on-a-chip for ultrafast manipulation of 350-MHz hard X-ray pulses. *Opt. Express* **29**, 13624 (2021).
- Park, J. et al. Laser-induced patterning for a diffraction grating using the phase change material of Ge₂Sb₂Te₅ (GST) as a spatial light modulator in X-ray optics: a proof of concept. *Opt. Mater. Express* **12**, 1408 (2022).
- Vaskivskiy, I. et al. Controlling the metal-to-insulator relaxation of the metastable hidden quantum state in 1T-TaS₂. *Sci. Adv.* **1**, e1500168 (2015).
- Okamoto, K. et al. Carrier dynamics in InGaN/GaN SQW structure probed by the transient grating method with subpicosecond pulsed laser. *Phys. Status Solidi B* **228**, 81–84 (2001).
- Ebihara, M., Sohn, W. Y. & Katayama, K. Lifetime mapping of photo-excited charge carriers by the transient grating imaging technique for nano-particulate semiconductor films. *Rev. Sci. Instrum.* **90**, 073905 (2019).
- Rasool, S. et al. Determination of carrier lifetime in thermally evaporated In₂S₃ thin films by light induced transient grating technique. *Appl. Phys. A* **126**, 312 (2020).
- Kading, O. W., Skurk, H., Maznev, A. A. & Matthias, E. Transient thermal gratings at surfaces for thermal characterization of bulk materials and thin films. *Appl. Phys. Mater. Sci. Process.* **61**, 253–261 (1995).

10. Vega-Flick, A. et al. Thermal transport in suspended silicon membranes measured by laser-induced transient gratings. *AIP Adv.* **6**, 121903 (2016).
11. Tobey, R. I. et al. Transient grating measurement of surface acoustic waves in thin metal films with extreme ultraviolet radiation. *Appl. Phys. Lett.* **89**, 091108 (2006).
12. Zoubková, K., Stoklasová, P., Grabec, T., Sedlák, P. & Seiner, H. Transient grating spectroscopy for complete elastic anisotropy: beyond the measurement of surface acoustic waves. In *2021 IEEE International Ultrasonics Symposium (IUS) 1–3* (IEEE, 2021); <https://doi.org/10.1109/IUS52206.2021.9593394>
13. Katayama, K., Shen, Q., Toyoda, T. & Nelson, K. A. Phonon polariton generation and detection using near-field heterodyne transient grating method. *Appl. Phys. Lett.* **90**, 171117 (2007).
14. Kawashima, H., Sasaki, F., Kobayashi, S. & Tani, T. Excitation of phonon-polaritons with asymmetric transient grating. *Jpn. J. Appl. Phys.* **36**, 6764–6767 (1997).
15. Gedik, N., Orenstein, J., Liang, R., Bonn, D. A. & Hardy, W. N. Transient gratings formed by nonequilibrium quasiparticles in $\text{YBa}_2\text{Cu}_3\text{O}_{6.5}$. *J. Supercond.* **17**, 117–120 (2004).
16. Tomoda, K., Adachi, S., Muto, S. & Shimomura, S. Transient grating studies of phase and spin relaxations of excitons in GaAs single quantum wells. *Phys. E* **42**, 2714–2717 (2010).
17. Janušonis, J. et al. Transient grating spectroscopy in magnetic thin films: simultaneous detection of elastic and magnetic dynamics. *Sci Rep.* **6**, 29143 (2016).
18. Wang, G. et al. Gate control of the electron spin-diffusion length in semiconductor quantum wells. *Nat. Commun.* **4**, 2372 (2013).
19. Bencivenga, F. et al. Four-wave mixing experiments with extreme ultraviolet transient gratings. *Nature* **520**, 205–208 (2015).
20. Foglia, L. et al. First evidence of purely extreme-ultraviolet four-wave mixing. *Phys. Rev. Lett.* **120**, 263901 (2018).
21. Bencivenga, F. et al. Nanoscale transient gratings excited and probed by extreme ultraviolet femtosecond pulses. *Sci. Adv.* **5**, eaaw5805 (2019).
22. Sezerman, O., Simpson, A. M. & Jericho, M. H. Thermal expansion of 1T-TaS₂ and 2H-NbSe₂. *Solid State Commun.* **36**, 737–740 (1980).
23. Gerasimenko, Y. A., Karpov, P., Vaskivskiy, I., Brazovskii, S. & Mihailovic, D. Intertwined chiral charge orders and topological stabilization of the light-induced state of a prototypical transition metal dichalcogenide. *npj Quantum Mater.* **4**, 32 (2019).
24. Gerasimenko, Y. A. et al. Quantum jamming transition to a correlated electron glass in 1T-TaS₂. *Nat. Mater.* **18**, 1078–1083 (2019).
25. Ravnik, J. et al. Quantum billiards with correlated electrons confined in triangular transition metal dichalcogenide monolayer nanostructures. *Nat. Commun.* **12**, 3793 (2021).
26. Foglia, L. et al. Extreme ultraviolet transient gratings: a tool for nanoscale photoacoustics. *Photoacoustics* **29**, 100453 (2023).
27. Stojchevska, L. et al. Ultrafast switching to a stable hidden quantum state in an electronic crystal. *Science* **344**, 177–180 (2014).
28. Eichberger, M. et al. Snapshots of cooperative atomic motions in the optical suppression of charge density waves. *Nature* **468**, 799–802 (2010).
29. Svetin, D. et al. Transitions between photoinduced macroscopic quantum states in 1T-TaS₂ controlled by substrate strain. *Appl. Phys. Express* **7**, 103201 (2014).
30. Le Guyader, L. et al. Stacking order dynamics in the quasi-two-dimensional dichalcogenide 1T-TaS₂ probed with MeV ultrafast electron diffraction. *Struct. Dyn.* **4**, 044020 (2017).
31. Stahl, Q. et al. Collapse of layer dimerization in the photo-induced hidden state of 1T-TaS₂. *Nat. Commun.* **11**, 1247 (2020).
32. Li, W. & Naik, G. V. Light-induced reorganization of charge density wave stacking in 1T-TaS₂. *Appl. Phys. Lett.* **118**, 253104 (2021).
33. Harvey, J. E. & Pfisterer, R. N. Understanding diffraction grating behavior, part II: parametric diffraction efficiency of sinusoidal reflection (holographic) gratings. *Opt. Eng.* **59**, 1 (2020).
34. Henke, B. L., Gullikson, E. M. & Davis, J. C. *X-ray Interactions: Photoabsorption, Scattering, Transmission, and Reflection at E=50–30,000eV, Z=1–92*, Atomic Data and Nuclear Data Tables (1993).
35. Maznev, A. A. et al. Generation and detection of 50 GHz surface acoustic waves by extreme ultraviolet pulses. *Appl. Phys. Lett.* **119**, 044102 (2021).
36. Mraz, A. et al. Charge configuration memory devices: energy efficiency and switching speed. *Nano Lett.* **22**, 4814–4821 (2022).
37. Wang, X. et al. Chemical growth of 1T-TaS₂ monolayer and thin films: robust charge density wave transitions and high bolometric responsivity. *Adv. Mater.* **30**, 1800074 (2018).
38. Enomoto, H., Kawano, T., Kawaguchi, M., Takano, Y. & Sekizawa, K. Van der Waals growth of thin TaS₂ on layered substrates by chemical vapor transport technique. *Jpn. J. Appl. Phys.* **43**, L123 (2004).
39. Lin, H. et al. Scanning tunneling spectroscopic study of monolayer 1T-TaS₂ and 1T-TaSe₂. *Nano Res.* **13**, 133–137 (2020).
40. Ziebeck, K. R. A., Dorner, B., Stirling, W. G. & Schollhorn, R. Kohn anomaly in the 1T₂ phase of TaS₂. *J. Phys. F* **7**, 1139–1143 (1977).

Publisher's note Springer Nature remains neutral with regard to jurisdictional claims in published maps and institutional affiliations.

Open Access This article is licensed under a Creative Commons Attribution 4.0 International License, which permits use, sharing, adaptation, distribution and reproduction in any medium or format, as long as you give appropriate credit to the original author(s) and the source, provide a link to the Creative Commons license, and indicate if changes were made. The images or other third party material in this article are included in the article's Creative Commons license, unless indicated otherwise in a credit line to the material. If material is not included in the article's Creative Commons license and your intended use is not permitted by statutory regulation or exceeds the permitted use, you will need to obtain permission directly from the copyright holder. To view a copy of this license, visit <http://creativecommons.org/licenses/by/4.0/>.

© The Author(s) 2024

Methods

Materials

The single-crystalline 1T-TaS₂ samples were grown using the chemical vapour transport method from elemental tantalum and sulfur, with iodine as a transport agent²⁷. The bulk crystals were exfoliated by the scotch tape technique and immediately inserted into the vacuum chamber to avoid oxidation. X-ray diffraction confirmed the high quality of the samples. Direct current transport measurements were performed for the initial characterization of the samples.

EUV transient grating experimental set-up

The experimental set-up is shown schematically in Fig. 1a. The transient grating experiments were performed at the EIS-TIMER beamline at the FERMI FEL facility (Triste) in backward diffraction geometry; -50 fs EUV pulses from the FEL source were split by the wavefront division beam splitters into two pump beams and one probe beam. After spectral filtering, the beams were overlapped and focused on the sample, which was mounted on a cold finger cryostat. The angle between the two pump beams was set to 27.6°, resulting in an interference pattern on the sample surface with a period of 87 nm, taking into account the pump wavelength $\lambda_{\text{pump}} = 39.9$ nm. The state of the sample was then monitored as a function of the time delay between the pumps and the probe in a stroboscopic manner, by recording the intensity of diffracted probe beam ($\lambda_{\text{probe}} = 13.3$ nm) with the charge-coupled device camera. For studying metastable structures at low temperatures, the sample was excited by a train of -50 pump pulses once (corresponding to 1 s illumination time), and then the slow dynamics was monitored in real time by repeatedly exposing the sample to the probe beam only. The incident fluence on the sample was 3.5 mJ cm⁻² for the probe beam and 3.8 mJ cm⁻² for each of the pump beams.

An energy-level diagram showing the pumping and probing transitions is illustrated in Fig. 1e. The pump photon energy $\hbar\omega_{\text{pump}} = 31.1$ eV is close to several electronic transitions in 1T-TaS₂ (ref. 41) from initial states of tantalum, whose binding energies are 34.7 (2) eV (O₃ edge 5p_{3/2}), 25.5 (1.7) eV (N₆ edge 4f_{5/2}) and 23.6 (1.2) eV (N₇ edge 4f_{7/2}) to tantalum 5d_{xy}, 5d_{3z²-1} final states (with bandwidth ≈ 2 eV) near the Fermi level; the full-width at half-maximum (in electron volts) are indicated in brackets. The probe wavelength $\hbar\omega_{\text{probe}} = 93.3$ eV is non-resonant and has at least a three-times-longer absorption length, which ensures that it does not disturb the grating despite the relatively high incident fluence used in the experiment.

The experiments were performed at room temperature (in the nearly commensurate state) and 100 K (in the commensurate ground state).

Fitting procedure

The room-temperature data was fitted as a superposition of exponential background and two damped oscillators:

$$I_{\text{TG}}(t) = I_0 H(t) (1 - e^{-t/\tau_0}) [I_1 e^{t/\tau_1} \sin(\omega_1 t + \varphi_1) + I_2 e^{t/\tau_2} \sin(\omega_2 t + \varphi_2) + I_3 e^{t/\tau_3}]$$

where I_n are amplitudes of individual components, $\omega_{1,2}$, $\varphi_{1,2}$, $\tau_{1,2}$ are the frequencies, phases and damping constants of the oscillators, respectively, and τ_3 is the relaxation time of the exponential background. Additional exponent with the characteristic time τ_0 was used to account for the rise time of the signal. As the FEL pulse length is much shorter than the relevant timescales, we assumed instantaneous excitation, which was modelled by a Heaviside function $H(t)$.

Data availability

The data used in this study are available from the corresponding author on reasonable request.

Code availability

The codes that support the findings of this study are available from the corresponding author on reasonable request.

References

- Ettema, A. R. H. F. & Haas, C. An X-ray photoemission spectroscopy study of interlayer charge transfer in some misfit layer compounds. *J. Phys. Condens. Matter* **5**, 3817–3826 (1993).

Acknowledgements

We are grateful for the support from the Slovenian Research and Innovation Agency (through program P1-0040 and grant nos. PR-08972, PR-10496 and PR-11213 to A.M., R.V. and G.J., respectively), the Slovene Ministry of Science (grant no. Raziskovalci-2.1-IJS-952005 to I.V.), and the European Union's Horizon 2020 research and innovation program under the Marie Skłodowska-Curie (grant agreement no. 860553 to E.P.). We wish to thank P. Sutar for providing the samples.

Author contributions

I.V., A.M., R.V., G.J., Y.V., R.C., F.P., L.F., D.A., J.P.C., E.P. and D.F. performed transient grating experiments. I.V., C.M. and D.M. devised the experiments. I.V., A.M., R.V., G.J., Y.V. and D.M. performed the analysis. I.V. and D.M. wrote the paper. I.V. led the experimental team. All authors contributed to revising the paper.

Competing interests

The authors declare no competing interests.

Additional information

Correspondence and requests for materials should be addressed to Igor Vaskivskyi.

Peer review information *Nature Photonics* thanks the anonymous reviewers for their contribution to the peer review of this work.

Reprints and permissions information is available at www.nature.com/reprints.